scientific reports

OPEN

A biomechanical model for concomitant functioning of neck and shoulder: a pilot study

Alexandra Yurova[1]✉, Andrey Gladkov[3,4], Eugene Kalinsky[2], Alexey Lychagin[2], Anatoly Shipilov[2] & Yuri Vassilevski[1,2,3]

A combination of pain syndromes in the neck and shoulder joints creates a significant burden on the healthcare system and has important social and economic significance. Treatment of these pathologies is often inefficient and can reduce the quality of life for patients. Studying of the relationship between pathological changes in the cervical spine and diseases of the shoulder area is crucial for developing more efficient treatment methods. Biomechanical modeling can be a valuable tool in this research, as assessing muscle function in patients is not always feasible. To our knowledge, there are no open-source biomechanical models for concomitant functioning of neck and shoulder. The aim of this research is to construct a biomechanical model for neck and shoulder concomitant functioning and to investigate numerically the work of neck and shoulder muscles during head and arm movements.

According to the International Association for the Study of Pain (IASP), 20 to 50% of the world's population suffers from pain in the neck and shoulder joints, while a combination of these pain syndromes is observed in 10% of cases[1,2]. The high prevalence (15-30%) of pain in the cervical-brachial complex among the working population aged 30-50 years creates a significant burden on the healthcare system and has important social and economic significance[3,4].

The shoulder joint is a crucial part of the upper limb movement mechanism, formed by the head of the humerus and the glenoid of the scapula. It is also a part of a shoulder girdle complex that includes the glenohumeral, acromioclavicular, sternoclavicular, and scapulothoracic joints[5,6]. Together, these joints ensure precise and efficient movements of the upper limb. Another important motor unit of the upper half of the human body is the cervical spine. It provides support and movement for the head while protecting the spinal cord, spinal nerves, and the vertebral arteries that supply blood to the brain[7,8]. However, due to its anatomical features, the cervical spine is extremely vulnerable. Weakness in the neck muscles increases the risk of cervical spine injury[9].

Pathology of the proximal part of the shoulder, the shoulder joint itself, and the shoulder girdle is a common and serious problem in orthopedics and traumatology[10]. It is well known that there is a close biomechanical connection between the spine and the upper limb girdle. In the vast majority of cases, patients with symptoms originating from both these locations simultaneously, are observed[11–13]. Treatment of this pathology is often inefficient and can reduce significantly the quality of life for patients. The current evidence is insufficient to state clearly the relationship between pathological changes in the cervical spine and the consequences of injuries and diseases of the shoulder area. Studying of this relationship is crucial for developing more efficient treatment methods[14,15]. The cervical spine and the shoulder girdle are closely connected anatomically and functionally, with dysfunction in one area often leading to compensatory changes in the other. Pathological changes in the cervical spine can often manifest as symptoms in the shoulder girdle, and vice versa. For example, a herniated disc in the cervical spine may lead to referred pain in the shoulder or arm, while shoulder impingement syndrome can cause neck pain and stiffness. By understanding how these structures interact with and influence each other, healthcare providers can better diagnose and treat patients with complex musculoskeletal issues.

Furthermore, research of the relationship between the cervical spine and shoulder girdle can help to identify common patterns of dysfunction that may be present in certain patient populations. This knowledge can inform the development of targeted rehabilitation programs that address both areas simultaneously, leading to more comprehensive and successful outcomes for patients. Studying this relationship can also have implications for injury prevention and performance optimization, particularly in athletes and individuals engaged in physical

[1]Marchuk Institute of Numerical Mathematics, Russian Academy of Sciences, 8 Gubkin str., Moscow 119333, Russia. [2]Sechenov University, 8-2 Trubetskayai str., Moscow 119991, Russia. [3]Moscow Institute of Physics and Technology, 9 Institutsky Lane, Dolgoprudny, Moscow Region 141700, Russia. [4]Present address: Skolkovo Institute of Science and Technology, The Territory of the Skolkovo Innovation Center, Bolshoy Boulevard, 30, bld. 1, Moscow 121205, Russia. ✉email: alexandra.yurova@gmail.com

activities. By identifying risk factors associated with dysfunction in the cervical spine and shoulder girdle, healthcare providers can develop strategies to mitigate these risks and improve overall musculoskeletal health. By unraveling the complex interplay between the cervical spine and the shoulder girdle, researchers and healthcare providers can enhance diagnostic accuracy, treatment efficacy, and overall quality of life for individuals with musculoskeletal conditions.

Biomechanical modeling can serve as an additional research tool. Currently, there are freely available biomechanical models that include independent representations of the neck[16–18] and shoulder[19–22]. To our knowledge, there are no open-source biomechanical models for concomitant functioning of neck and shoulder. In our study, we focus on traumatic causes of cervical-shoulder syndrome (domestic, sports, road traffic), which can be primarily represented in the biomechanical model through such structures as bones and muscles. Soft tissues and skin may not require such detailed consideration in this instance. The aim of this research is to construct a biomechanical model for neck and shoulder concomitant functioning and to investigate numerically the work of neck and shoulder muscles during head and arm movements. The proposed model was developed using data from a healthy volunteer; however, it can be adapted for other patients by adjusting the anthropometric and muscular parameters. The model can be used for forward modeling with the aim of pathology research. We impose certain restrictions for patients whose pathologies may be reproduced by such model: adult patients of working age with no prior history of pain or dysfunction in the neck, shoulder girdle, or upper limb before the injury. Patients with prior diseases of the cervical spine and upper limbs that required targeted specialized treatment do not meet our inclusion criteria.

Methods

The main steps of this study are as follows: construction of the biomechanical model for neck and shoulder concomitant functioning, carrying out a motion capture experiment for head and arm movements, adjustment of model parameters and computation of muscle contribution to the movements. The developed biomechanical model was created based on the core principles of multibody systems, which are widely used for modeling of rigid bodies interactions[23]. The basic components of the multibody systems are:

- Rigid bodies with mass and inertia properties (bones);
- Connections that constrain relative motion between bodies (joints);
- Force elements (springs, dampers, actuators that apply forces);
- Kinematic constraints (mathematical relationships defining allowable motions).

The interactions between bodies can involve both kinematic (motion-related) and dynamic (force-related) analyses. In our research, we focus on both kinematics (to reproduce the necessary neck and shoulder motions in the model) and dynamics (to examine the forces and moments that lead to motion). Details on the principles of kinematic analysis are presented in Section "Motion capture experiment", description of a muscle function as a force element is provided in Section "Adjustment of model parameters", and methods for performing dynamic analysis are described in Section "Computation of muscle contribution to the movements".

Construction of the biomechanical model for neck and shoulder concomitant functioning

To construct the biomechanical model with the required design, we used the open-source platform OpenSim[24–26], developed for biomechanical modeling of various systems and processes, such as shoulder, neck, knee, and ankle joints[16,22,27,28], as well as assistive devices[29]. To simplify the process of model construction, some elements of the model were borrowed from existing freely available models: the thoracolumbar spine and ribcage model[17], shoulder model with an accurate scapulothoracic joint[22], musculoskeletal model of head and neck[30]. The thoracolumbar spine and ribcage model includes a fully articulated thoracolumbar spine, with 3 rotational degrees-of-freedom at each inter-vertebral joint, and a ribcage. The model also contains muscle representations, which parameters were adjusted to match a community-based sample of 125 datasets obtained from in vivo computed tomography scans. The shoulder model includes the major muscles of the ribcage and scapula, specifying kinematics of the latter. The neck model was developed by incorporating hyoid muscles to existing neck models to reproduce realistic movement in all directions. We used some components from these models to construct the model for neck and shoulder concomitant functioning. Firstly, the masses, inertia properties and movement constraints for vertebrae C1-C7 were taken from the neck model to replace a unified body with separate vertebrae. Secondly, the representations of the acromioclavicular and sternoclavicular joints were borrowed from the shoulder model, since they are presented in more detail and better describe scapular and clavicular kinematics. For our research, it is particularly important that implementation of this joint allows us to perform modeling of such movements as shoulder elevation, abduction, and flexion while maintaining scapular movement close to reality. The shoulder model assumes the movement of a specific point on the scapula along an ellipsoidal surface. The joint frame origin of the scapula on the ellipsoid fixed to the parent thorax body is determined through a sequence of abduction (adduction) and elevation (depression) movements. Subsequently, the scapula undergoes rotational adjustments upward or downward around the normal to the surface, represented by the scapula Z-axis. Additionally, internal rotation, commonly known as "winging" is implemented as a positive rotation about the Y-axis within the scapular plane, maintaining tangency to the thoracic surface. The representation of scapulothoracic joint was included in the left and right sides of the model[22]. Thirdly, in addition to the muscles of the thoracolumbar spine and ribcage model (trapezius, serratus anterior, deltoid, supraspinatus, infraspinatus, subscapularis, teres minor, teres major, sternocleidomastoideus, longissimus, scalenus, longus colli), the muscles rhomboid, levator scapulae, obliqus capitis, rectus capitis (rf. Fig. 1) and latissimus dorsi were inserted to the model.

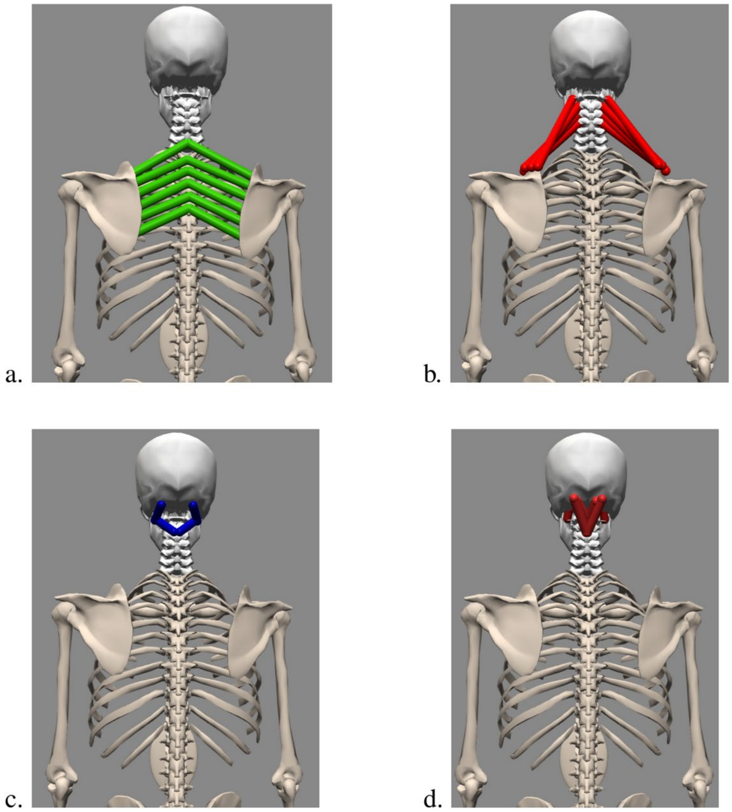

Fig. 1. New muscles added to the model: (**a**) Rhomboid; (**b**) Levator scapulae; (**c**) Obliqus capitis; (**d**) Rectus capitis.

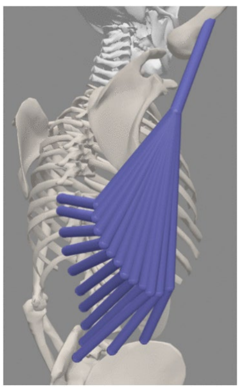

Fig. 2. The latissimus dorsi muscle during shoulder abduction (representation in the model).

The muscle shapes and attachment points have been determined in collaboration with orthopedists from Sechenov University. Basing on the anatomical similarity of the muscles, we adopted parameters for the new muscles from the thoracolumbar spine and ribcage model. Analogously, parameters for rhomboid and latissimus dorsi components were borrowed from trapezius, parameters for obliqus capitis and rectus capitis were taken from hyoid.

The latissimus dorsi muscle has a complex shape. The muscle architecture contains 12 components[31]. In addition to the origin and insertion points, the supplementary points are required to define the muscle's shape precisely and to avoid the use of wrapping objects[32], which slow down computations[33]. Figure 2 demonstrates the latissimus dorsi muscle during shoulder abduction.

The values of the tendon slack length and pennation angle for superior, middle and inferior components were borrowed from[22]. The correction of the deltoid muscle attachment point has been performed to prevent bone intersection during shoulder flexion (Fig. 3a,b).

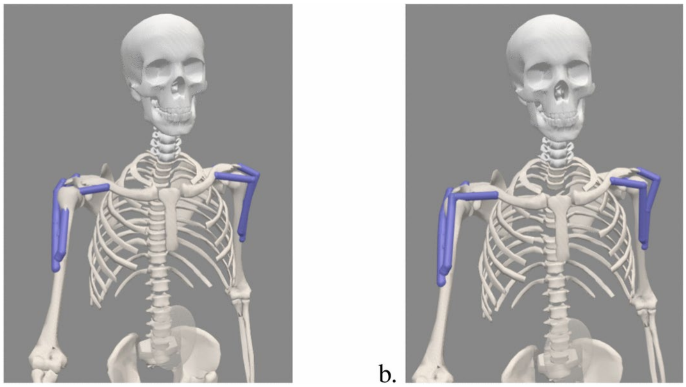

a. b.

Fig. 3. (**a**) Deltoid muscle intersecting humerus bone during shoulder flexion. (**b**) Deltoid muscle moving correctly during shoulder flexion.

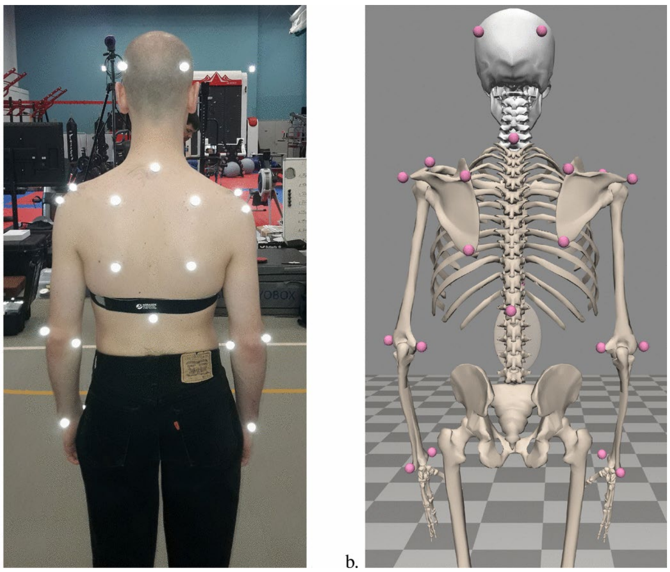

a. b.

Fig. 4. (**a**) Locations of experimental markers on the back of the subject. (**b**) Locations of the model markers.

Finally, all generalized coordinates, which do not relate to the motion of neck and shoulder, were frozen. The constructed model includes all main functional elements for studying the concomitant functioning of the shoulder and neck.

Motion capture experiment

The series of motion capture experiments has been carried out to record movements of head and arm. These experiments are necessary to obtain the dependence of generalized coordinates on time. The participant for the experiment was recruited during the period from 08.12.2022 to 18.09.2023 in accordance with the approval of the local ethics committee of Sechenov University. The participant provided verbal informed consent, which was witnessed by other participants of the study who are co-authors of this article. The subject is a healthy 25-year-old male with mass 66 kg and height 180 cm. A special marker positioning protocol was developed in accordance with the recommendations of the International Society of Biomechanics[34]. Figure 4a demonstrates the position of markers on the subject's back.

During the experiment, skin markers were placed on a thin volunteer with an asthenic body type, low body weight, and well-defined muscles. Markers were set on the prominent parts of the bones, with multiple markers placed on the same bone. This determined the accuracy of bone movement reproduction in the biomechanical model.

The total number of markers is 40. The recording of marker coordinates over time was conducted for shoulder flexion/extension, shoulder abduction/adduction, as well as head left turn and forward/backward/right tilt. The experiments were conducted for the movements of the right hand. During this work, we conducted multiple motion capture experiments to record the same movements. The volunteer is not able to reproduce the same movement absolutely accurately across different trials, but the general movement patterns are typically well replicated. The potential discrepancies among the results from motion capture experiments for the same movements are difficult to quantify, as the same movement may be performed over different time intervals in different trials, complicating the comparison of marker locations at various time steps. However, reproducing the overall motion pattern appears to be more important. We applied smoothing algorithms to all data collected from the motion capture experiments. The obtained data was analyzed in a system of coordinates associated with the human body with the origin in the center of mass of four relatively stable markers (C7, T8, IJ, PX). They are placed on spine and sternum and are almost motionless during the experiment (rf. Fig.5). This can be seen from small standard deviations of their coordinates.

Given this data, we perform the following stages for personalization of the biomechanical model:

- Scaling,
- Adjustment of scapulothoracic joint ellipsoid parameters.The scaling procedure was performed iteratively in the OpenSim GUI, to fit the model geometry to the subject sizes. Scaling implies changing the size of each body of the multibody system representing the subject's skeleton, along the axes X, Y, Z by a certain coefficient such that the model markers closely match the experimental ones. A proportional adjustment of masses, inertia tensors, and muscle attachment points of the scaled model is carried out. The original non-scaled model has a set of markers located in the same anatomical positions as the experimental markers (Fig. 4b).

To ensure the accurate representation of the scapulothoracic joint after scaling, it was necessary to adjust the parameters of the ellipsoid which restricts motion of the scapula. To determine the lengths of ellipsoid's semi-axes a, b, c and its barycenter x_0, y_0, z_0, we used the gradient descent method that minimizes residuals associated with the ellipsoid equation at each time step:

$$f(x_0, y_0, z_0, a, b, c) = \sum_t \left[\left(\frac{x(t) - x_0}{a} \right)^2 + \left(\frac{y(t) - y_0}{b} \right)^2 + \left(\frac{z(t) - z_0}{c} \right)^2 - 1 \right]^2 \longrightarrow \text{min},$$

where $x(t)$, $y(t)$, $z(t)$ are the coordinates of some scapula point at time t found experimentally.

Further, the Opensim Inverse Kinematics tool was applied. The values of generalized coordinates which place the geometrical model in a pose optimally corresponding to the experimental markers for each time step were determined. Achieving the "best match" involves solving the weighted least squares problem:

$$\min_{\mathrm{q}} \left[\sum_{i \in \text{markers}} \omega_i \|\mathrm{x}_i^{\text{exp}} - \mathrm{x}_i(\mathrm{q})\|^2 \right],$$

where q is the vector of generalized coordinates being solved for, $\mathrm{x}_i^{\text{exp}}$ is the position of marker i measured during the experiment, $\mathrm{x}_i(\mathrm{q})$ is the position of the corresponding model marker. During head movements, the marker weights ω_i were chosen to be equal, while during arm movements, a higher weight was assigned to the scapula markers. Specifically, the weights assigned to the scapula markers were set to 2,3,6, to the elbow markers to 2, while those assigned to the other markers were set to 1.

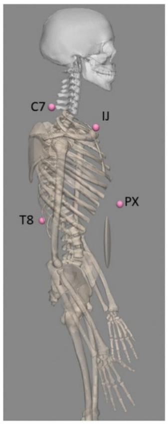

Fig. 5. Markers C7, T8, IJ, PX used to compute the origin of the coordinate system associated with the human body.

Adjustment of model parameters

Adjusting parameters is one of the key stages in constructing of a biomechanical model. In this study, parameter setting was performed for the resting position, attempting to simulate the basic postural tone, *i.e.* the minimal continuous muscle activity required to maintain the subject's posture at the standing position. This muscle activity is essential for providing stability and preventing the body from collapsing[35]. The basic postural tone is expressed in terms of muscle model parameters. The Hill-type muscle model used in OpenSim is described in[36]. Muscles are presented as a set of fibers which attach to tendon at pennation angle α. The muscle fiber consists of two elements: a contractile element and a parallel elastic element in series with an elastic tendon. The contractile element and the parallel elastic element correspond to active and passive muscle forces. The schematic view of the pasive, active and total force-length curves corresponding to the Hill-type models is shown in Fig. 6a. The active force length curve of the Millard muscle model is demonstrated in Fig. 6b.

The tendon slack length and the pennation angle parameters for each muscle were determined by adjustment (after scaling) of the muscle parameters in the initial model. The muscle fiber length l^M in the standing position is

$$l^M = \frac{l^{MT} - l_s^T}{cos\alpha},$$

where l^{MT} is the length of the muscle-tendon complex, l_s^T is the tendon slack length, α is the pennation angle. The optimal fiber length parameter is defined by

$$l_{opt} = \frac{l^M}{l_{max}^M k},$$

where k is the coefficient determining the initial muscle tension, l_{max}^M is the maximum active normalized fiber length equal to 1.8123 in Millard muscle model[37].

The above parameter determination establishes small initial tensions in the neck and shoulder muscles which correspond to the basic postural tone. We automated the parameter adjustment using Python-version of the OpenSim library.

Computation of muscle contribution to the movements

Once the muscle parameters are adjusted and the generalized coordinates q are determined for each particular movement, one can find individual muscle forces and muscle activations which bring the model to the desired positions at any time moment, for each particular movement. Each movement is governed by the multibody dynamics equation

$$M(\mathrm{q})\ddot{\mathrm{q}} = \mathrm{C}(\mathrm{q}, \dot{\mathrm{q}}) + \mathrm{G}(\mathrm{q}) + \mathrm{F}, \tag{1}$$

where $\mathrm{q}(t), \dot{\mathrm{q}}(t), \ddot{\mathrm{q}}(t)$ are generalized coordinates, velocity and acceleration, correspondingly, $\mathrm{C}(\mathrm{q}, \dot{\mathrm{q}})$ is the Coriolis and centrifugal forces term, $\mathrm{G}(\mathrm{q})$ is the gravity force, and F denotes other forces applied to the model. The OpenSim Static Optimization Tool exploits known movement of the model and the solution of equation (1) in order to determine unknown generalized forces (such as joint torques) by minimizing the objective function

$$J = \sum_{m=1}^{n} a_m^2 \longrightarrow \min \tag{2}$$

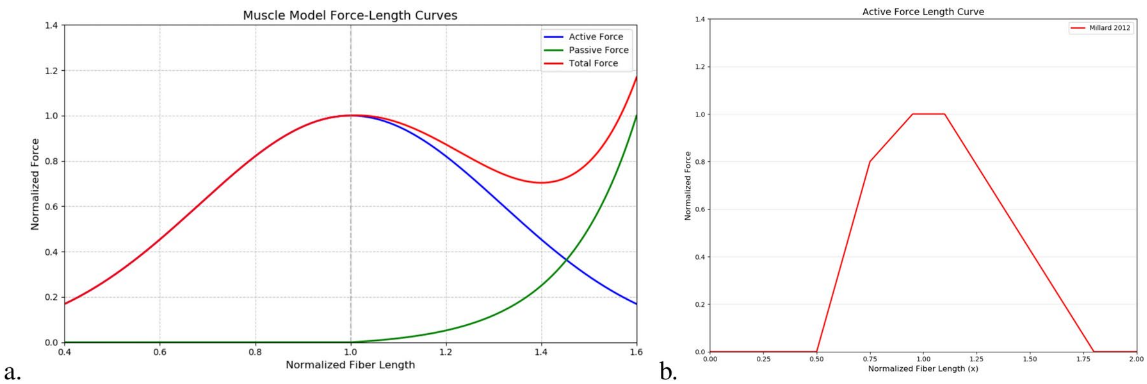

Fig. 6. (**a**) The schematic view of the pasive, active and total force-length curves corresponding to the Hill-type models. (**b**) The active force length curve of the Millard muscle model.

under the constraint:

$$\sum_{m=1}^{n}\left[a_m f(F_m^0, l_m, v_m)\right] r_{m,j} = \tau_j.$$

Here for the *j* joint axis $r_{m,j}$ is the moment arm of muscle *m* about the axis and τ_j is the generalized force acting about the axis; *n* is the number of muscles involved in the model, $a_m = a_m(t)$ is the activation level of muscle *m* at discrete time step, F_m^0 is the maximum isometric force of muscle *m*, l_m is the length of muscle *m*, v_m is the shortening velocity of muscle *m*, $f(F_0^m, l_m, v_m) = F_0^m f^L(l_m^M) f^V(v_m^M)$ is a force-length-velocity surface of muscle *m*, where $f^L(l_m^M)$ and $f^V(v_m^M)$ are the active-force–length and force–velocity curves.

With chosen muscle parameters, the solution of the static optimization problem may fail for some movements, as the model is not entirely anatomically accurate. For the sake of robustness of the solution, we included into the model coordinate actuators for each unlocked coordinate following[26]. The primary role of the coordinate actuator is to compute and apply forces $f(t) = f^{opt}\xi(t)$ and their moments to the associated bodies based on its control function $\xi(t)$ and the model's current state. The optimal actuator force f^{opt} is a user-defined parameter. Actuator action is essential to compensate inaccuracies in motion capture measurements, muscle structure, and parameter selection. However, during movement execution, the action of actuators should be reduced. To avoid excessive usage of actuators during motion execution, it is crucial to minimize the optimal actuator force f^{opt}: higher values f^{opt} can exert a significant impact even with low values of $\xi(t)$. At the same time, the action of the actuators should be sufficient to enable the execution of the movement. We attempted to find the minimum value of optimal actuator force at which the Static Optimization problem could be solved. For the head movements we set $f^{opt} = 0.1$ N, for the arm movements we set $f^{opt} = 1.0$ N.

Results

Model construction and movement reproduction

The obtained results of scaling procedure match the error range presented in the results evaluation guide[38]: the root mean square error is 1.5 cm, the maximum error is 2.6 cm, where error is the distance between an experimental marker and the corresponding marker on the model. Changes in anthropometric properties are illustrated in Fig. 7.

The final model for neck and shoulder concomitant functioning contains 23 muscles (Fig. 8).

We recorded movements of the head and the right arm of the subject using the motion capture technology for subsequent reproduction by the model. Due to the large number of markers, achieving accuracy within the specified error range from[38] for all markers was challenging. Generalized coordinates bringing the model into the specified position at each time moment were determined using the Inverse Kinematics algorithm[25]. The reproduced movements are shown in Fig. 9. All the muscles did not intersect the bones during all the examined movements.

Table 1 presents the errors of the Inverse Kinematics algorithm for the investigated movements. According to[38], maximum marker error should generally be less than 2-4 cm and the RMS under 2 cm.

Model sensitivity analysis

We analyzed the model's sensitivity to the parameter *k*, which determines the initial tension in the muscles. We performed experiments with the parameter value decreased and increased by 5 percent relative to the main experiment. In Fig. 10 we provide force computation results for different neck and head muscle components, including both the left and right muscles, for turning head to the left.

In Fig. 11 we provide force computation results for the same neck and head muscle components, for shoulder flexion. The model appears to be relatively robust to parameter changes, but shows increased sensitivity to the parameter *k* for periods of intense muscle activation.

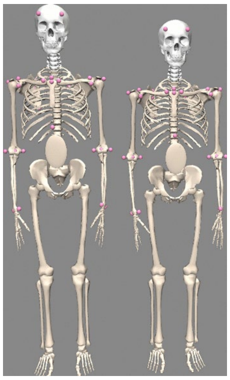

Fig. 7. Initial model (left) and model after scaling (right).

a. b.

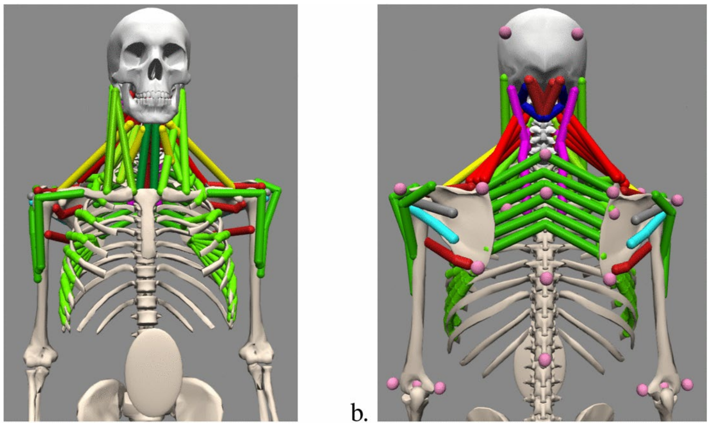

Fig. 8. Front (**a**) and back (**b**) views of the model (some muscles are hidden).

We also performed the model sensitivity analysis regarding muscle maximal isometric force F_m^0, varying its values by 5 percent relative to the initial experiment. The results are presented in Figs. 12 and 13. The results for the model sensitivity analysis regarding tendon slack length l_s^T, varying its values by 5 percent relative to the initial experiment are presented in Figs. 14 and 15. The sensitivity to parameters F_m^0 and l_s^T appears to be low.

Muscles contributions to the movements

For each movement the work of a muscle is given by:

$$W = \int_{t_0}^{t_1} F \frac{dl^M}{dt} dt,$$

where t_0, t_1 are the start and the end time of the movement, *F* is the muscle force along the tendon and l^M is the muscle fiber length. Computed changes of force and length for the trapezius muscle component attached to clavicle during the arm abduction are presented in Fig. 16.

Basing on the computed work for each muscle, we generated a pie chart illustrating the contribution of muscles during each movement. The computed contributions of muscles to the head movements (turning the head to the left and the forward/backward/right head tilt) are presented in Fig. 17, the computed contributions of muscles to the shoulder movements (flexion/extension, abduction and shrug) are illustrated in Fig. 18.

Table 2 demonstrates computed positive work (in Joules) of different muscles during flexion.

Discussion

In this paper we presented the new biomechanical model for neck and shoulder concomitant functioning. The model contains 23 muscles and 142 muscle components. In Table 3 we summarize the key features of the model which enable realistic reproduction of neck and shoulder movements for further investigations. To the best of our knowledge, there is currently no open-access biomechanical model that provides a detailed representation of the functionalities of the neck and shoulder girdle.

Data of the motion capture analysis and personalization of the biomechanical model provide estimation of muscle contributions to the movements of interest. The primary objective of our study at this stage was a qualitative reproduction of the muscle functionality in the model. Validation of the computed contribution is hampered by the lack of instruments estimating forces and activations of deep muscles during movement. To our knowledge, only a few studies reproduce arm movements using biomechanical modeling and provide results on the muscle contribution.

The computed muscle contributions obtained for head movements as well as for shoulder flexion qualitatively align with anatomical data and information from medical practice. In each of the four movements, both shoulder and neck muscles are involved. The computed muscle contributions for the shoulder shrug, flexion and abduction can be compared with[22]. Both studies demonstrate significant role of the trapezius and deltoid muscles in flexion and abduction, as well as of the levator scapulae in shrugging. However, our study demonstrated major impact of shoulder muscles infraspinatus and supraspinatus in flexion and abduction. The differences can be explained by differences in model architectures, in particular in muscle modeling approaches (attachment points locations, muscle structure, parameters), e.g. trapezius muscle in our model is presented using more muscle components, which do not intersect scapula. The model[22] contains mainly shoulder and back muscles, whereas in our model we introduce many neck muscles. Table 2 demonstrates that the muscle work performed during shoulder flexion is distributed among a greater number of muscles than in[22] and also done by neck and back muscles. The total work in our model is lower in our study, which may be attributed to the fact that only the arm lifting phase was

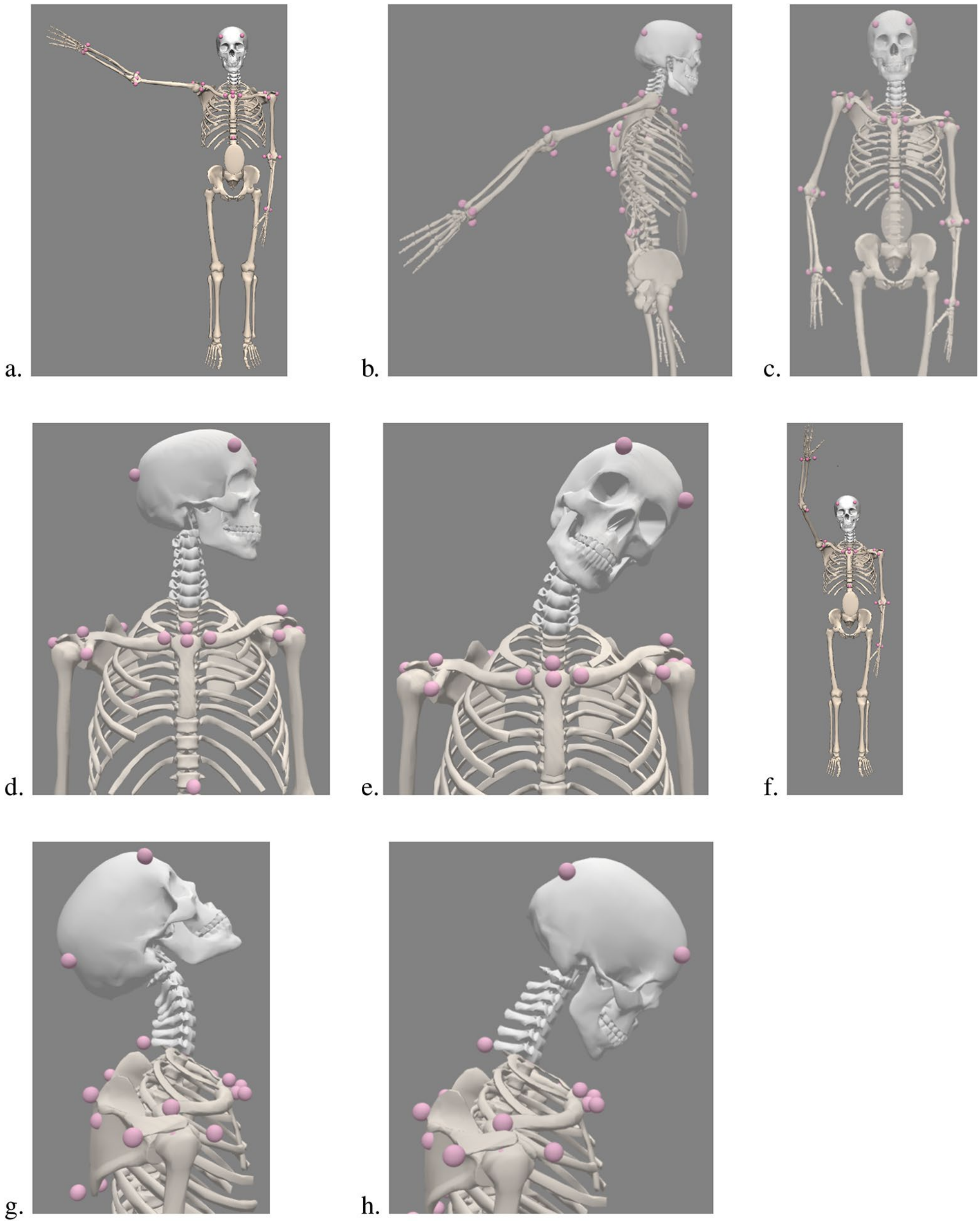

Fig. 9. Movements recorded during motion capture experiment: (**a**) Shoulder abduction. (**b**) Shoulder extension. (**c**) Shoulder shrug. (**d**) Turning head to the left. (**e**) Head tilt to the left. (**f**) Shoulder flexion. (**g**) Backward head tilt. (**h**) Forward head tilt.

considered, as well as potential differences in flexion speed in both studies. In study[22], OpenSim Computed Muscle Control algorithm was used to compute muscle forces during movements.

On the other hand, the computed muscle contributions for flexion and extension deviate from expected outcomes stemming from the anatomical knowledge. This difference is the consequence of limitations of this study:

- The motion capture markers are placed on the skin and may capture movements of the skin, rather than movements of the bones beneath it. This limitation is particularly evident when one tries to capture motion of the scapula, the most actively moving bone during shoulder movements. Alternative algorithms are required for better detection of movements for some bones such as scapula;
- The static optimization computes the active fiber force along the tendon under assumption that tendons are rigid and do not include contribution from muscles' parallel elastic element. To obtain more realistic results, it is necessary to use alternative algorithms for calculating muscle forces, *e.g.* the OpenSim Computed Muscle Control Algorithm;
- Representation of muscle attachment points and muscle parameters, including initial tensions in the standing pose, is not precise. These parameters are highly personalized and their estimation is prone to have er-

Movement	RMS, m	max, m
Turning head to the left	0.015	0.026
Forward head tilt	0.014	0.026
Backward head tilt	0.015	0.025
Head tilt to the right	0.014	0.026
Shoulder flexion	0.023	0.040
Shoulder extension	0.017	0.037
Shoulder abduction	0.021	0.039
Shoulder shrug	0.020	0.039

Table 1. RMS and max errors of the Inverse Kinematics algorithm for different movements.

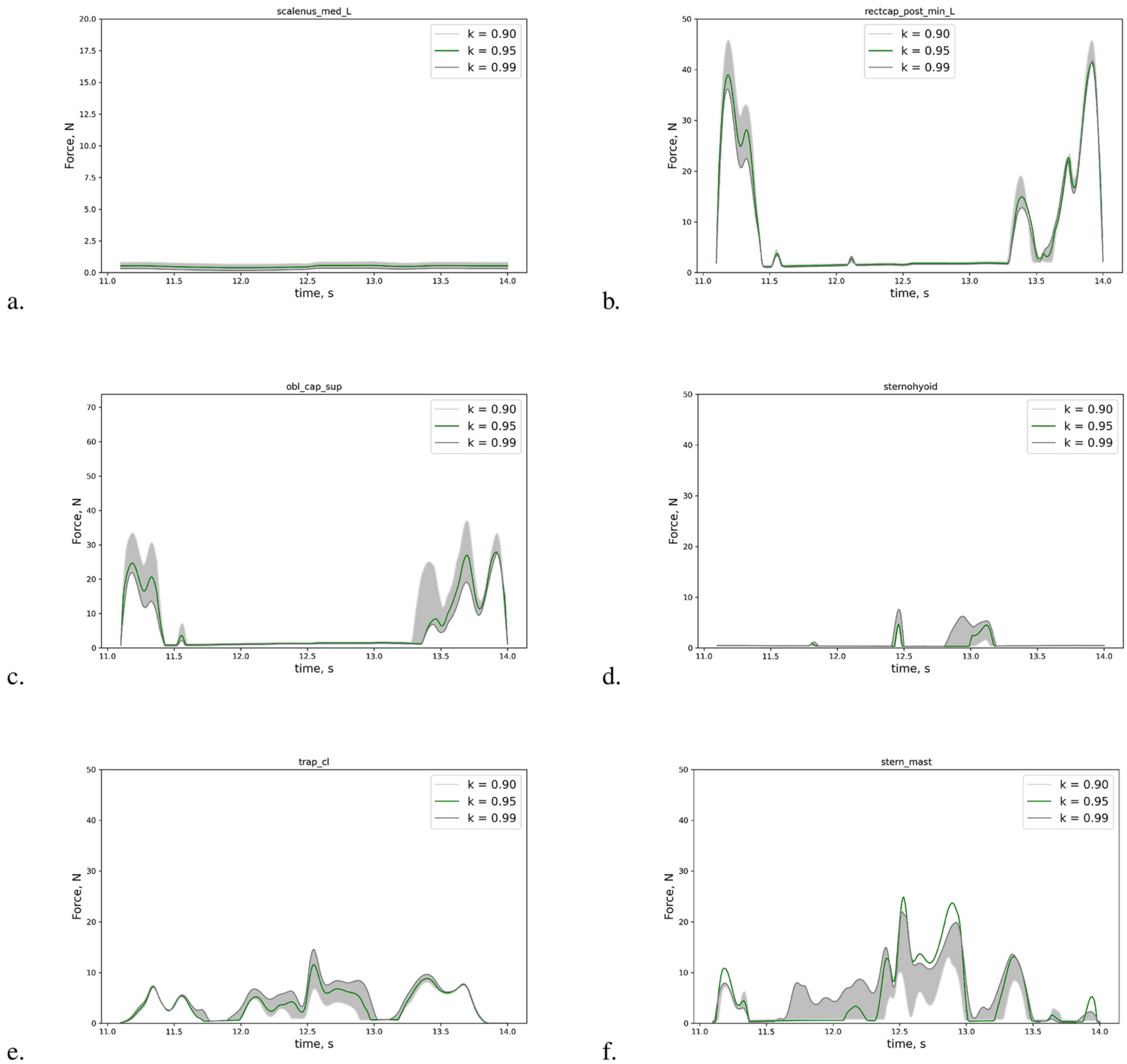

Fig. 10. Results of force computation for neck and head muscles with different initial tension for turning head to the left: (**a**) Scalenus medius. (**b**) Rectus capitis posterior major. (**c**) Obliquus capitis superior. (**d**) Sternohyoid. (**e**) Trapezius muscle, upper fibers. (**f**) Sternocleidomastoideus.

rors.Quantifying the impact of these limitations is challenging. A separate study is necessary to investigate the influence of algorithmic errors in inverse kinematics and the positioning of attachment points on calculation results. By now, there are only a few studies providing quantitative estimations of the differences in results from OpenSim Computed Muscle Control and Static Optimization algorithms. For instance, in[39], such results for the lower extremity are presented. To our knowledge, there are no analogous data for the muscles of the neck, back, and head.

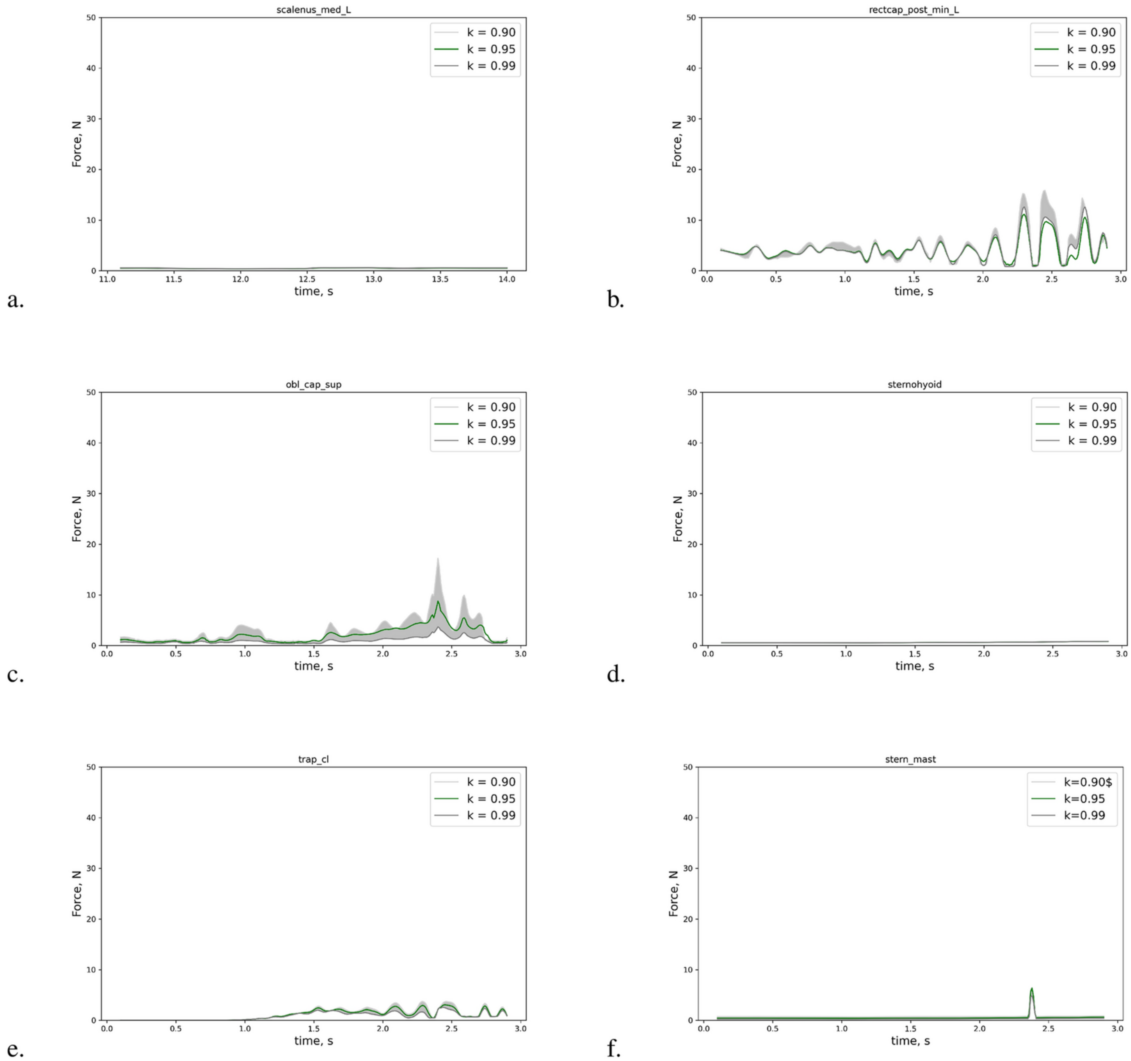

Fig. 11. Results of force computation for neck and head muscles with different initial tension for shoulder flexion: (**a**) Scalenus medius. (**b**) Rectus capitis posterior major. (**c**) Obliquus capitis superior. (**d**) Sternohyoid. (**e**) Trapezius muscle, upper fibers. (**f**) Sternocleidomastoideus.

We note that the existing open-access data primarily involves numerical analysis of muscle forces produced during shoulder movements, which has mostly been conducted on simpler models and considers fewer movements[22]. In contrast, our analysis explores multiple movements on the basis of a more elaborated model, providing a novel contribution. We evaluate the results based on the accurate reproduction of kinematics, anatomically consistent parameter settings, and the model's robustness with respect to crucial parameters.

Conclusion

In this study, the biomechanical model for concomitant neck and shoulder normal functioning was presented.

The novelty of this research is as follows:

- A model for the concomitant functioning of the neck and shoulder has been developed, which includes the necessary functionality for realistic reproduction of neck and shoulder movements, as well as numerical analysis of movement characteristics;
- The movements of turning the head to the left, head tilt to the left, backward and forward head tilt, shoulder abduction, shoulder flexion and extension, and shoulder shrug were recorded using motion capture technology and reproduced on the developed model with accuracy that meets accepted standards;
- Muscle contributions to the recorded neck and shoulder movements have been computed.

The proposed model was developed using data from a healthy volunteer; however, it can be adapted for other patients by adjusting the anthropometric and muscular parameters. The model can be used for forward modeling with the aim of pathology research.

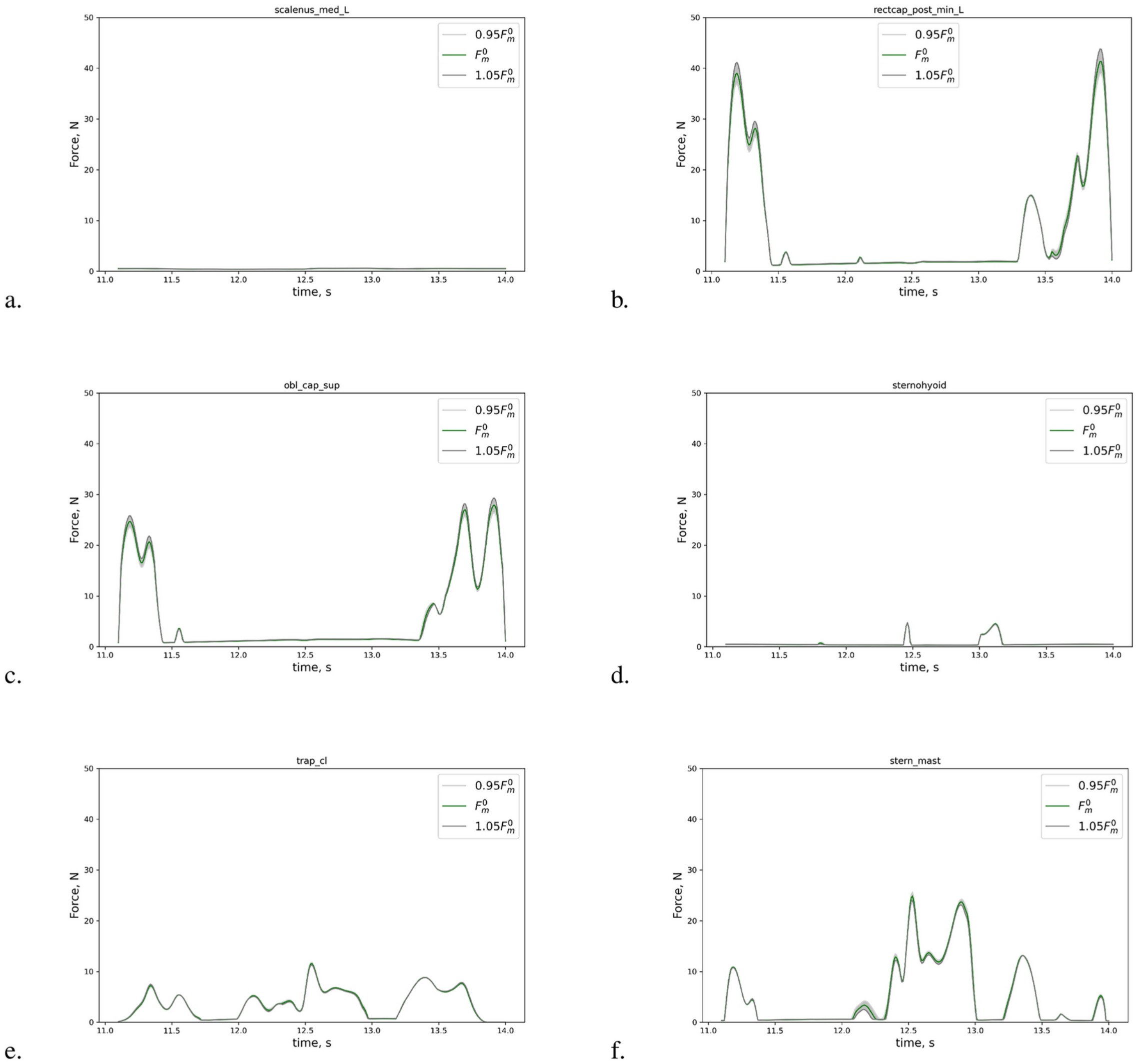

Fig. 12. Results of force computation for neck and head muscles with different maximal isometric forces for turning head to the left: (**a**) Scalenus medius. (**b**) Rectus capitis posterior major. (**c**) Obliquus capitis superior. (**d**) Sternohyoid. (**e**) Trapezius muscle, upper fibers. (**f**) Sternocleidomastoideus.

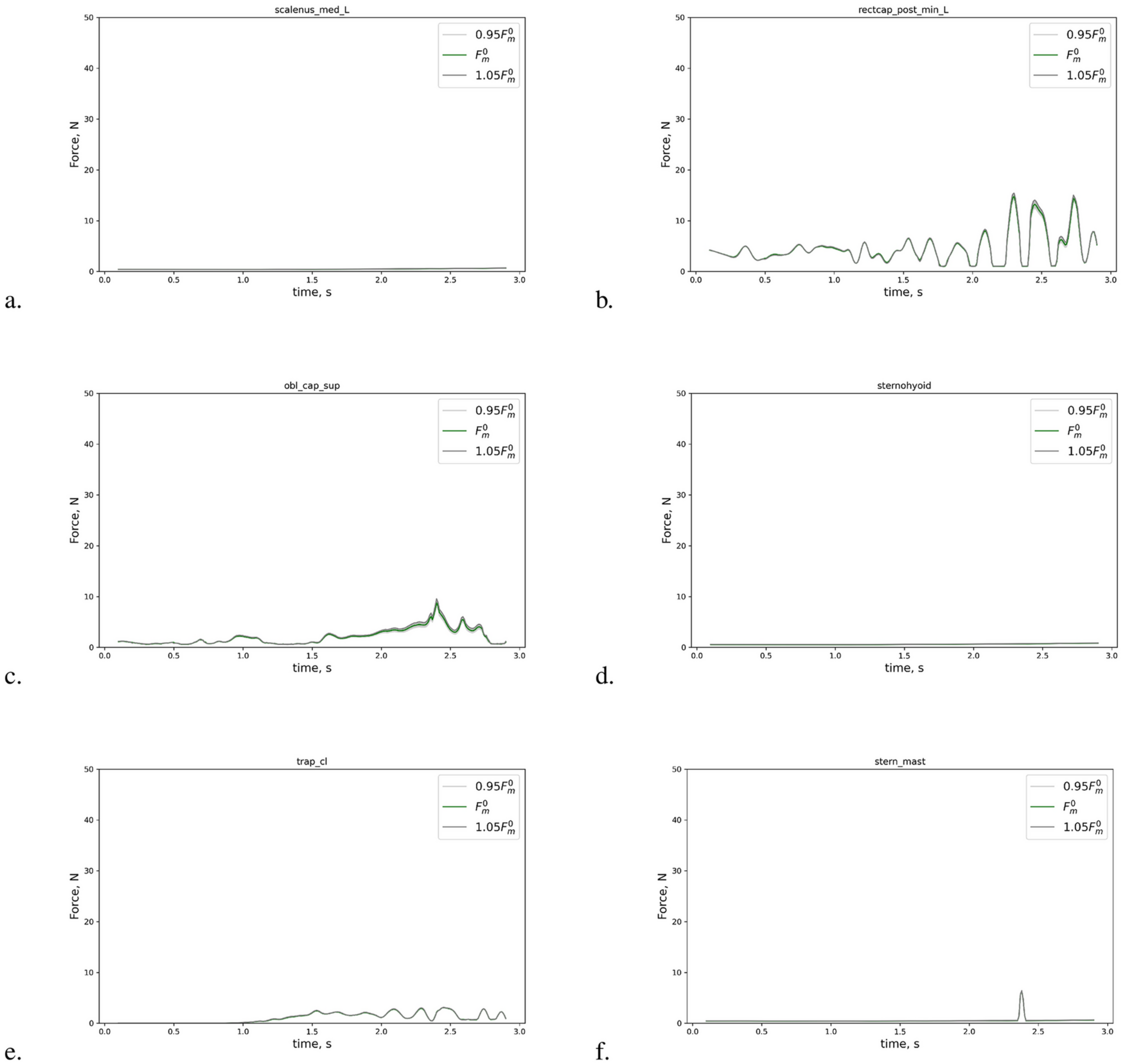

Fig. 13. Results of force computation for neck and head muscles with different maximal isometric forces for shoulder flexion: (**a**) Scalenus medius. (**b**) Rectus capitis posterior major. (**c**) Obliquus capitis superior. (**d**) Sternohyoid. (**e**) Trapezius muscle, upper fibers. (**f**) Sternocleidomastoideus.

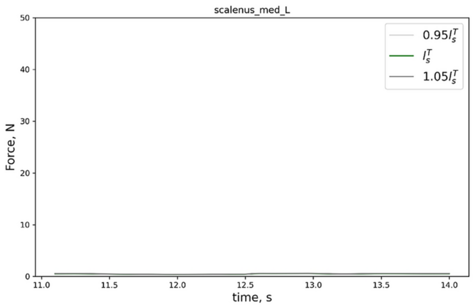

a.

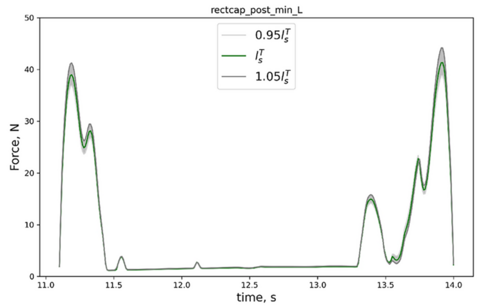

b.

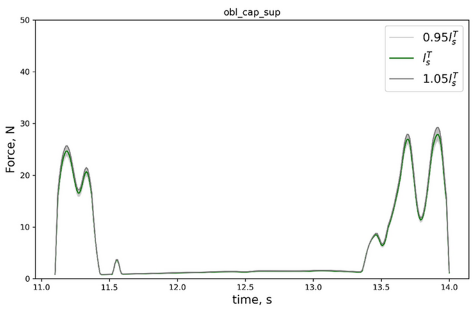

c.

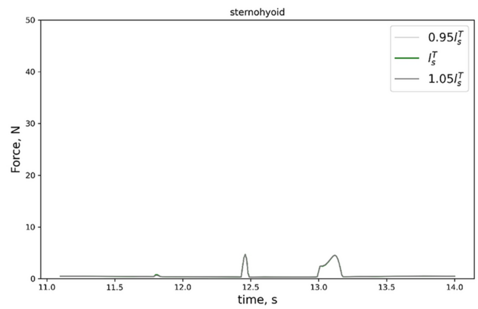

d.

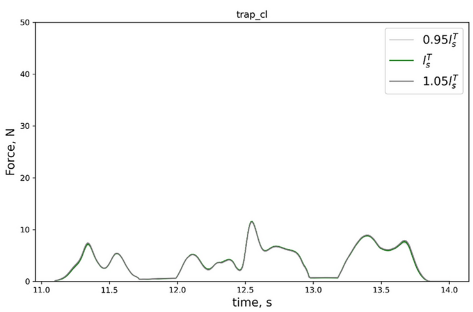

e.

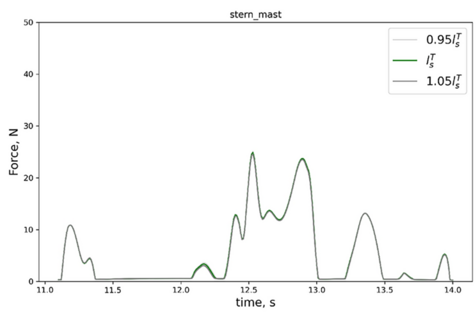

f.

Fig. 14. Results of force computation for neck and head muscles with different tendon slack lengths for turning head to the left: (**a**) Scalenus medius. (**b**) Rectus capitis posterior major. (**c**) Obliquus capitis superior. (**d**) Sternohyoid. (**e**) Trapezius muscle, upper fibers. (**f**) Sternocleidomastoideus.

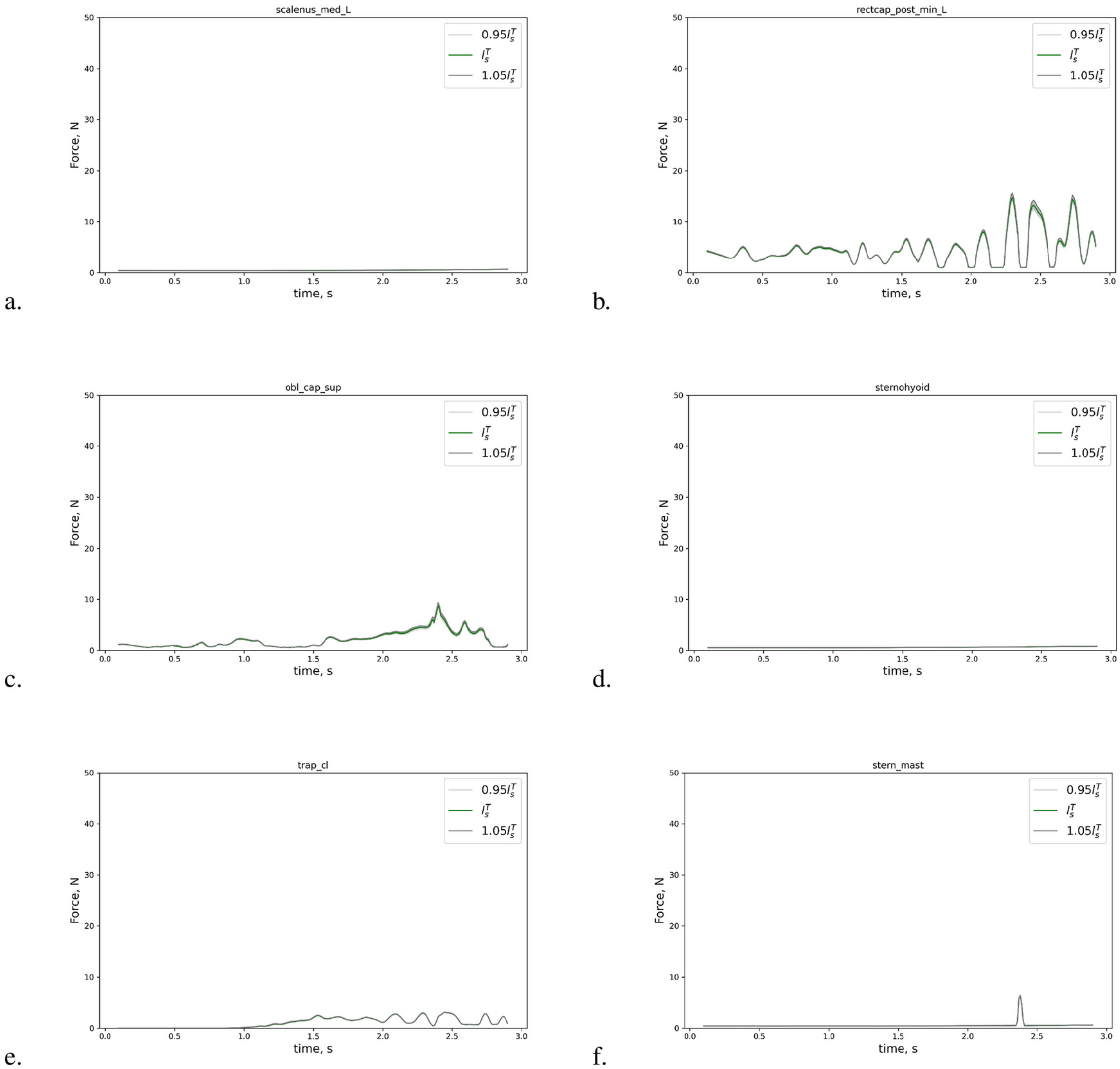

Fig. 15. Results of force computation for neck and head muscles with different tendon slack lengths for shoulder flexion: (**a**) Scalenus medius. (**b**) Rectus capitis posterior major. (**c**) Obliquus capitis superior. (**d**) Sternohyoid. (**e**) Trapezius muscle, upper fibers. (**f**) Sternocleidomastoideus.

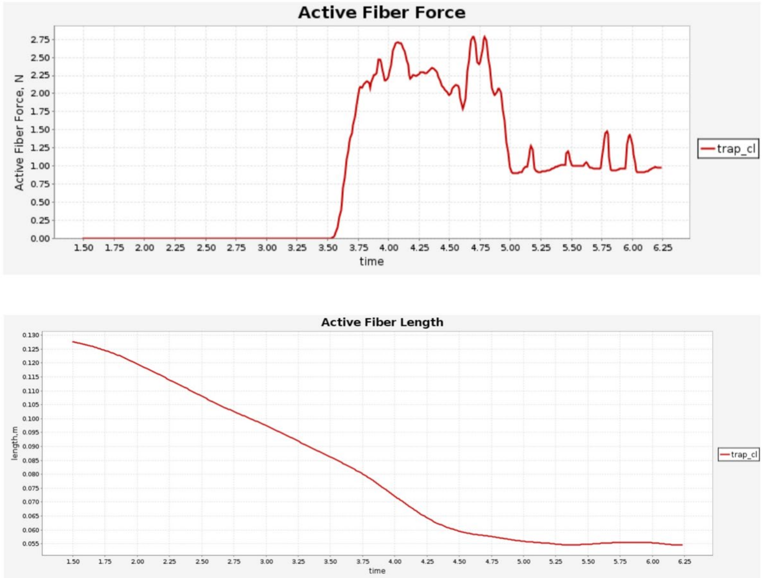

Fig. 16. Force (**a**) and length (**b**) of trapezius component during arm abduction.

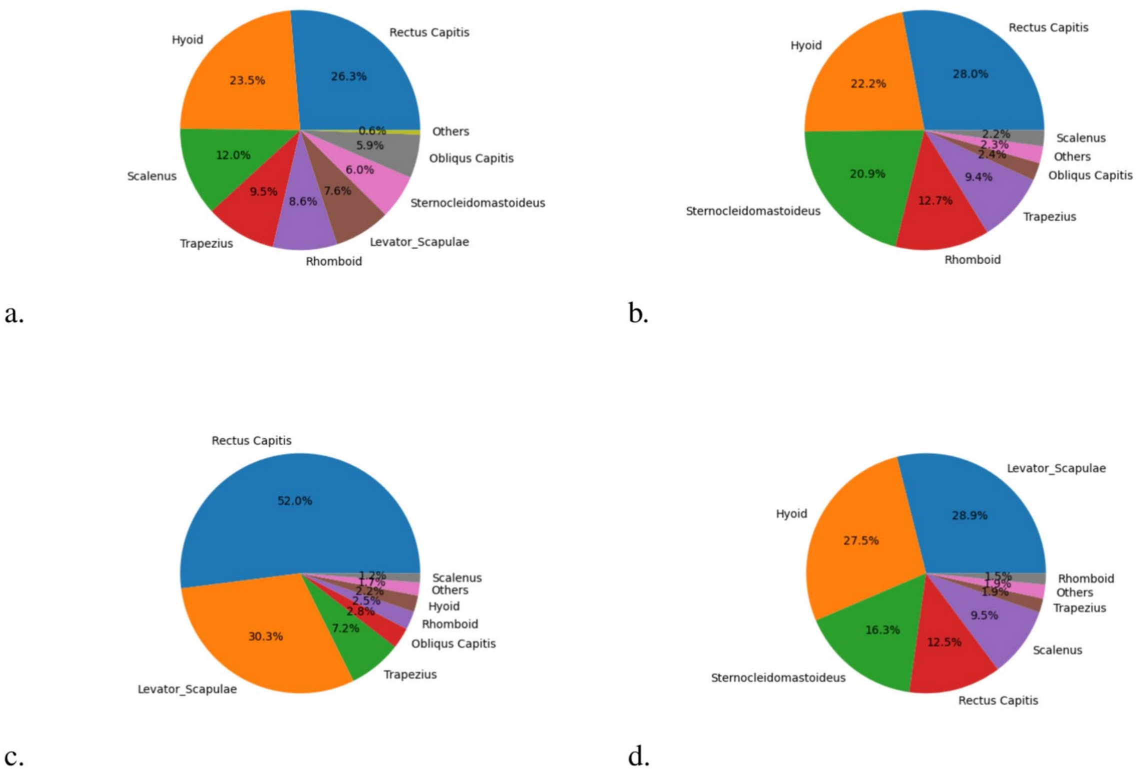

Fig. 17. Muscle work contribution for the head movements: (**a**) Turning head to the left. (**b**) Forward head tilt. (**c**) Backward head tilt. (**d**) Head tilt to the right.

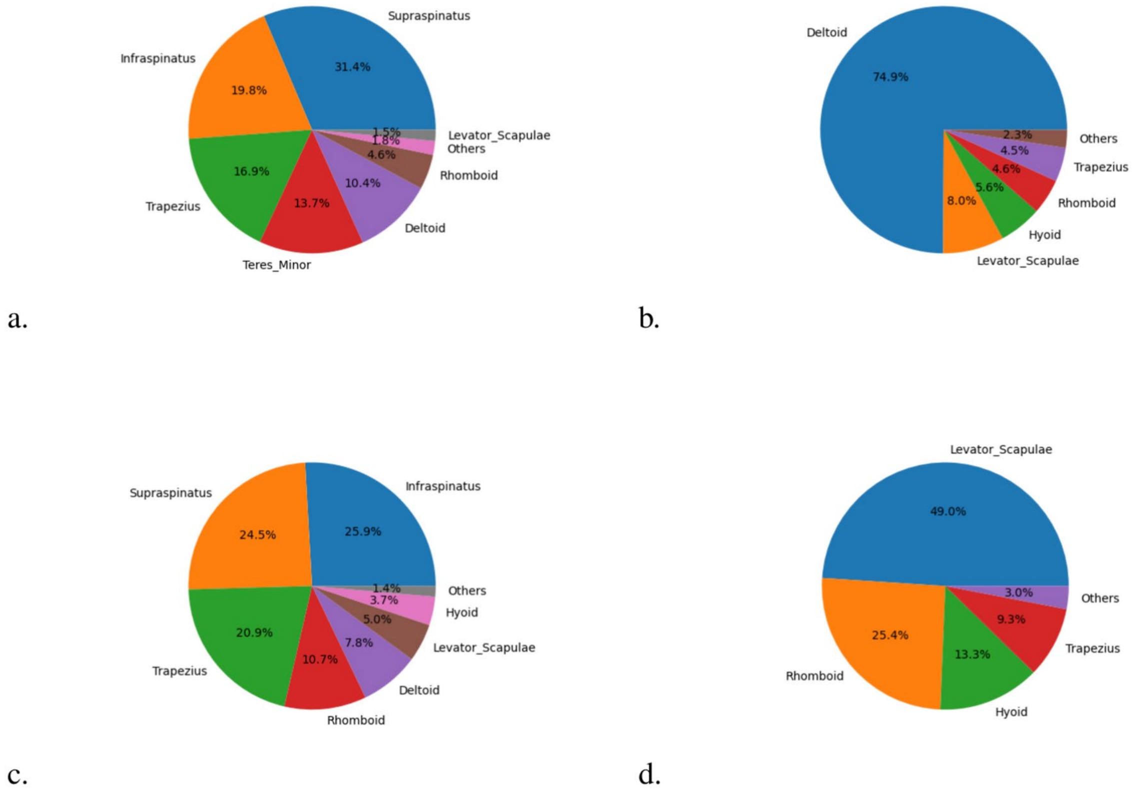

Fig. 18. Muscle work contribution for the right arm movements: (**a**) Shoulder flexion. (**b**) Shoulder extension. (**c**) Shoulder abduction. (**d**) Shoulder shrug.

Muscle	Work, Joules
Supraspinatus	2.844
Infraspinatus	1.793
Trapezius	1.531
Teres minor	1.238
Deltoid	0.945
Rhomboid	0.415
Levator scapulae	0.132

Table 2. Positive work (J) done by the muscles during shoulder flexion.

Implemented feature	Function
Separated vertebrae with constraints on the relative movement	Model allows to represent the motions of the neck with 6 degrees of freedom for vertebrae
Sternoclavicular joint (movements of the clavicle relative to the sternum)	
Acromioclavicular joint (movements of the clavicle relative to the acromion)	Allow for elevation, depression, protraction, retraction, and rotation
Scapulothoracic joint (movement of the scapula over the rib cage)	
Neck muscles (levator scapulae, sternocleidomastoideus, sternohyoideus, omohyoideus, rectus capitis lateralis, rectus capitis posterior major, rectus capitis posterior minor, obliquus capitis superior, obliquus capitis inferior, obliquus capitis inferior, obliquus capitis superior, scalenus posterior, scalenus medius, scalenus anterior, longissimus cervicis, longissimus capitis, longus capitis, longus colli)	Provide stability and control for neck motion, supporting head position and facilitating movements in multiple directions
Shoulder muscles (serratus anterior, rhomboideus, deltoideus, teres major, infraspinatus, teres minor, subscapularis, supraspinatus)	Enable a wide range of shoulder movements, including flexion, extension, abduction, and rotation of the arm
Back muscles (trapezius, latissimus dorsi)	Assist in movements of the shoulders and arms
Markers	Allow for scaling the model to account for the anthropometric data of individual subjects and reproducing the subjects' movements on the model based on motion capture experiments data; the markers are aligned with commonly accepted international protocols
Actuators	Allow for compensating model inaccuracies, enabling the reproduction of real movements

Table 3. Key features of the developed biomechanical model for concomitant functioning of neck and shoulder.

Data availability

The biomechanical model for neck and shoulder concomitant functioning and motion capture data are freely available for download at https://simtk.org/projects/neck_shoulder.

Received: 6 June 2024; Accepted: 11 December 2024
Published online: 30 December 2024

References

1. Simon, J. et al. Is there a neck-shoulder syndrome?. *Glob. J. Anesth. Pain Med.* **1**(1), 1–5 (2019).
2. Pribicevic, Mario. The Epidemiology of Shoulder Pain: A Narrative Review of the Literature. https://doi.org/10.5772/52931 (2012).
3. Peshkova, M. et al. Gender-related aspects in osteoarthritis development and progression: A review. *Int. J. Mol. Sci.* **23**(5), 2767. https://doi.org/10.3390/ijms23052767 (2022).
4. Safiri, S. et al. Global, regional, and national burden of neck pain in the general population, 1990–2017: Systematic analysis of the Global Burden of Disease Study 2017. *BMJ* **26**(368), m791. https://doi.org/10.1136/bmj.m791 (2020).
5. Bakhsh, W. & Nicandri, G. Anatomy and physical examination of the shoulder. *Sports Med. Arthrosc. Rev.* **26**(3), e10–e22. https://doi.org/10.1097/JSA.0000000000000202 (2018).
6. Lugo, R., Kung, P. & Ma, C. B. Shoulder biomechanics. *Eur. J. Radiol.* **68**(1), 16–24. https://doi.org/10.1016/j.ejrad.2008.02.051 (2008).
7. Kazeminasab, S. et al. Neck pain: Global epidemiology, trends and risk factors. *BMC Musculoskelet. Disord.* **23**(1), 26. https://doi.org/10.1186/s12891-021-04957-4 (2022).
8. Côté, P., Cassidy, D. J., Carroll, L. J. & Kristman, V. The annual incidence and course of neck pain in the general population: A population-based cohort study. *Pain* **112**(3), 267–273. https://doi.org/10.1016/j.pain.2004.09.004 (2004).
9. Ribeiro, D. C. et al. The prevalence of myofascial trigger points in neck and shoulder-related disorders: A systematic review of the literature. *BMC Musculoskelet. Disord.* **19**(1), 252. https://doi.org/10.1186/s12891-018-2157-9 (2018).
10. Andersen, L. L. et al. A randomized controlled intervention trial to relieve and prevent neck/shoulder pain. *Med. Sci. Sports Exerc.* **40**(6), 983–90. https://doi.org/10.1249/MSS.0b013e3181676640 (2008).
11. Badcock, L. J., Lewis, M., Hay, E. M. & Croft, P. R. Consultation and the outcome of shoulder-neck pain: A cohort study in the population. *J. Rheumatol.* **30**(12), 2694–9 (2003).
12. Manifold, S. G. & McCann, P. D. Cervical radiculitis and shoulder disorders. *Clin. Orthop. Relat. Res.* **368**, 105–13 (1999).
13. Gheysvandi, E. et al. Neck and shoulder pain among elementary school students: Prevalence and its risk factors. *BMC Public Health* **19**, 1299. https://doi.org/10.1186/s12889-019-7706-0 (2019).
14. Iaroshevskyi, O. A., Morozova, O. G., Logvinenko, A. V. & Lypynska, Y. V. Non-pharmacological treatment of chronic neck-shoulder myofascial pain in patients with forward head posture. *Wiad. Lek.* **72**(1), 84–88 (2019).
15. Pateder, D. B., Berg, J. H. & Thal, R. Neck and shoulder pain: Differentiating cervical spine pathology from shoulder pathology. *J. Surg. Orthop. Adv.* **18**(4), 170–4 (2009).
16. Roos, P. E., Vasavada, A., Zheng, L. & Zhou, X. Neck musculoskeletal model generation through anthropometric scaling. *PLoS ONE* **15**(1), e0219954. https://doi.org/10.1371/journal.pone.0219954 (2020).
17. Bruno, A. G., Bouxsein, M. L. & Anderson, D. E. Development and validation of a musculoskeletal model of the fully articulated thoracolumbar spine and rib cage. *J. Biomech. Eng.* **137**(8), 081003. https://doi.org/10.1115/1.4030408 (2015).
18. Cazzola, D., Holsgrove, T. P., Preatoni, E., Gill, H. S. & Trewartha, G. Cervical spine injuries: A whole-body musculoskeletal model for the analysis of spinal loading. *PLoS ONE* **12**(1), e0169329. https://doi.org/10.1371/journal.pone.0169329 (2017).
19. Holzbaur, K. R., Murray, W. M. & Delp, S. L. A model of the upper extremity for simulating musculoskeletal surgery and analyzing neuromuscular control. *Ann. Biomed. Eng.* **33**(6), 829–40 (2005).
20. Seth, A., Matias, R., Veloso, A.P. & Delp, S.L. A biomechanical model of the scapulothoracic joint to accurately capture scapular kinematics during shoulder movements. PLOS ONE (2015).
21. Nikooyan, A. A., Veeger, H. E., Chadwick, E. K., Praagman, M. & Helm, F. C. Development of a comprehensive musculoskeletal model of the shoulder and elbow. *Med. Biol. Eng. Comput.* **49**(12), 1425–35. https://doi.org/10.1007/s11517-011-0839-7 (2011).
22. Seth, A., Dong, M., Matias, R. & Delp, S. Muscle contributions to upper-extremity movement and work from a musculoskeletal model of the human shoulder. *Front. Neurorobot.* **5**(13), 90. https://doi.org/10.3389/fnbot.2019.00090 (2019).
23. Jason K. Moore. Learn Multibody Dynamics https://moorepants.github.io/learn-multibody-dynamics/learnmultibodydynamics.pdf.

24. Seth, A. et al. OpenSim: Simulating musculoskeletal dynamics and neuromuscular control to study human and animal movement. *PLoS Comput. Biol.* **14**(7), e1006223. https://doi.org/10.1371/journal.pcbi.1006223 (2018).
25. Delp, S. L. et al. OpenSim: Open-source software to create and analyze dynamic simulations of movement. *IEEE Trans. Biomed. Eng.* **54**(11), 1940–1950 (2007).
26. Seth, A., Sherman, M., Reinbolt, J. A. & Delp, S. L. OpenSim: A musculoskeletal modeling and simulation framework for in silico investigations and exchange. *Proc. IUTAM* **2**, 212–232 (2011).
27. Yurova, A. S. et al. Patellar motion and dysfunction of its stabilizers in a biomechanical model of the knee joint. *Sechenov Med. J.* **15**(1), 47–60. https://doi.org/10.47093/2218-7332.2024.15.1.47-60 (2024).
28. Maharaj, J. N. et al. Modelling the complexity of the foot and ankle during human locomotion: The development and validation of a multi-segment foot model using biplanar videoradiography. *Comput. Methods Biomech. Biomed. Engin.* **25**(5), 554–565. https://doi.org/10.1080/10255842.2021.1968844 (2022).
29. Dembia, C. L., Silder, A., Uchida, T. K., Hicks, J. L. & Delp, S. L. Simulating ideal assistive devices to reduce the metabolic cost of walking with heavy loads. *PLoS ONE* **12**(7), e0180320. https://doi.org/10.1371/journal.pone.0180320 (2017).
30. Mortensen, J. D., Vasavada, A. N. & Merryweather, A. S. The inclusion of hyoid muscles improve moment generating capacity and dynamic simulations in musculoskeletal models of the head and neck. *PLoS ONE* **13**(6), e0199912 (2018).
31. Netter, Frank H. Atlas of human anatomy. 6th Philadelphia, PA: Saunders/Elsevier, Text. (2014)
32. OpenSim User's Guide. Release 2.4. April 4, 2012. https://simtk-confluence.stanford.edu:8443/download/attachments/2624226/OpenSimUsersGuide04042012.pdf (Accessed on 21.11.2023).
33. Simulation with OpenSim - Best Practices. https://simtk-confluence.stanford.edu:8443/display/OpenSim/Simulation+with+OpenSim+-+Best+Practices (Accessed on 21.11.2023).
34. Wu, G. et al. International Society of Biomechanics. ISB recommendation on definitions of joint coordinate systems of various joints for the reporting of human joint motion–Part II: shoulder, elbow, wrist and hand. *J. Biomech.* **38**(5), 981–992. https://doi.org/10.1016/j.jbiomech.2004.05.042 (2005).
35. Ivanenko, Y. & Gurfinkel, V. S. Human postural control. *Front. Neurosci.* **20**(12), 171. https://doi.org/10.3389/fnins.2018.00171 (2018).
36. Zajac, F. E. Muscle and tendon: Properties, models, scaling, and application to biomechanics and motor control. *Crit. Rev. Biomed. Eng.* **17**, 359–411 (1989).
37. Millard, M., Uchida, T., Seth, A. & Delp, S. L. Flexing computational muscle: Modeling and simulation of musculotendon dynamics. *J. Biomech. Eng.* **135**(2), 021005. https://doi.org/10.1115/1.4023390 (2013).
38. OpenSim Advanced User & Developer Workshop. March 19-21, Stanford University (2012).
39. Roelker, Sarah et al. Effects of optimization technique on simulated muscle activations and forces. *J. Appl. Biomech.* **36**, 1–20. https://doi.org/10.1123/jab.2018-0332 (2020).

Author contributions
Conceptualization, Eugene Kalinsky and Alexey Lychagin; methodology, software, Andrey Gladkov and Alexandra Yurova; investigation — Anatoly Shipilov; writing—original draft preparation, Alexandra Yurova, Andrey Gladkov, Eugene Kalinsky; writing—review and editing, Yuri Vassilevski; administration, Alexandra Yurova; funding acquisition, Yuri Vassilevski. All authors reviewed the manuscript.

Funding
The authors wish to acknowledge financial support from the RSF grant No 21-71-30023.

Declarations

Competing interests
The authors declare no competing interests.

Additional information
Correspondence and requests for materials should be addressed to A.Y.

Reprints and permissions information is available at www.nature.com/reprints.

Publisher's note Springer Nature remains neutral with regard to jurisdictional claims in published maps and institutional affiliations.